Analyzing Dynamic Characteristics
of Working Rotor Pair in Vacuum Pumps

Nguyen Thanh Tung[1,2], Van-The Tran[1(✉)], and Do Anh Tuan[1]

[1] Department of Mechanical Engineering, Hung Yen University of Technology
and Education, 39 Road, Hung Yen City, Vietnam
vanct4.hut@gmail.com
[2] Ha Noi University of Mining and Geology, Ha Noi City, Vietnam

Abstract. The vacuum pumps are usually applied in many different life and industrial fields, such as food, medicine and biotechnology. They are used to convey various materials, from low viscosity fluids such as water to very high viscosity fluids such as oil, and even solids. The dynamic characteristics of a meshing rotor pair are greatly affect the working process of the vacuum pumps. In this paper, a method is presented to determine the dynamic characteristics of a meshing rotor pair in vacuum pump working process. The mathematical model and 3D CAD model of rotor pair are also constructed to perform analysis dynamic characteristics of rotor pair. The dynamic load of rotor is defined by the variable forces and variable stiffness of the system by using Adams software. The influence of rotational rotor speed on the dynamic load has been analyzed. Subsequently, the numerical results are presented to verify the merit of constructed model.

Keywords: Dynamic characteristic · Rotor pair · Vacuum pump

1 Introduction

The roots pumps are widely used in the life and industrial applications to transport with various materials including low and high viscosity fluids. The rotor's tooth profile is an important factor for improving performance of the vacuum pump. In this paper, a new tooth profile is designed based on the combination of the different traditional curves such as circular arc, extended epicycloid, involute curve.

The researches for improving rotor's tooth profile of vacuum pump have published in recently years. A tooth profile of a rotor is designed by using a single circular arc [1, 2]. A new tooth profile for rotor is proposed by combining circular arcs and a conjugated epicycloid [3]. A tooth profiles of rotor by comprising four circular arcs that can improve area efficiency of a vacuum pump patented by Fang [4]. Subsequently, Fong and Wang [5] have developed the tooth profile of the rotor that is combined by five circular arcs. For increasing pump efficiency, Niimura et al. [6] patented a tooth profile consisted a circular arc and an involute. For improving pump performance, Hwang and Hsieh [7, 8] have designed a tooth profiles using an extended cycloid curve with a variable trochoid ratio. And Kang et al. [9, 10] developed a new lobe pump rotor

profile used circular and epicycloid. A profile design of rotor consisting of a hypocycloid and epicycloid is presented by Chiu [11].

In this paper, based on the previous study [12], the tooth profile of CIC Roots rotors is composed of three curves which comprise orderly one circular arc on the rotor tooth tip, an involute and one conjugated circular arc in the root of rotor tooth. The tooth profile of EE Roots rotors is constructed by an extended epicycloid. 3D rotor models for both EE Roots rotors and CIC Roots rotors are constructed. Numeral example is presented to illustrate and verify that the CIC Roots rotors have more advances than the EE Roots rotors.

2 Mathematical Models for Generating Tooth Profiles of the Roots Rotors

2.1 CIC Tooth Profile

The CIC tooth profile is comprised by a circular arc (addendum portion A_1B_1), an involute curve (pitch circle portion B_1C_1) and a conjugated circular arc (dedendum portion C_1D_1), as shown in Fig. 1. The position locus tooth profiles of Roots rotor are represented in the coordinate system $S_1(x_1, y_1, z_1)$ as follows:

(1) The circular arc A_1B_1:

$$\mathbf{r}_{III_1}^{(A_1B_1)}(\ell) = \begin{cases} x_{III_1}^{(A_1B_1)}(\ell) = r_a \cos \ell \\ y_{III_1}^{(A_1B_1)}(\ell) = r_a \sin \ell \end{cases}, \quad (0 \leq \ell \leq \ell_1) \tag{1}$$

(2) The involute curve B_1C_1:

$$\mathbf{r}_{II_1}^{(B_1C_1)}(\ell) = \begin{cases} x_{II_1}^{(B_1C_1)}(\ell) = (r_p + \ell \cos \alpha_p) \cos \beta - \ell \cos \alpha_p \cot \alpha_p \sin \beta \\ y_{II_1}^{(B_1C_1)}(\ell) = \ell \cos(\beta - \alpha_p) \cot \alpha_p + r_p \sin \beta \end{cases}, \quad (-u \leq \ell \leq u) \tag{2}$$

with $\beta = \left(\frac{\pi}{2N} - \frac{\ell}{r_p \sin \alpha_p} \right)$

(3) The dedendum circular arc C_1D_1 can be obtained by rotating E_1F_1 (In Fig. 2) an angle of $\vartheta = \frac{(N-1)\pi}{N}$ counterclockwise about z axis:

$$\mathbf{r}_{II_1}^{(C_1D_1)}(\ell) = \begin{cases} x_{II_1}^{(C_1D_1)}(\ell) = 2r_p \cos(\vartheta - \ell) + r_a \cos(\vartheta + 3\ell) \\ y_{II_1}^{(C_1D_1)}(\ell) = 2r_p \sin(\vartheta - \ell) + r_a \sin(\vartheta + 3\ell) \end{cases}. \tag{3}$$
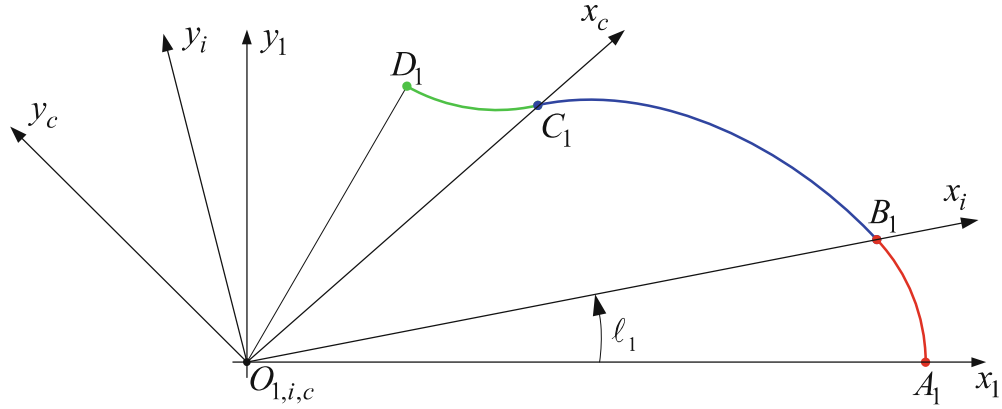
Fig. 1. The tooth profile of the CIC Roots rotors.

In Fig. 2(a), the meshing coordinate system for two Roots rotor is presented, the coordinate systems $S_1(x_1, y_1, z_1)$, $S_2(x_2, y_2, z_2)$, and $S_f(x_f, y_f, z_f)$ are rigidly connected to the driving rotor, the driven rotor, and the frame, respectively. By applying the homogeneous coordinate transformation matrix equation from $S_1(x_1, y_1, z_1)$ to $S_2(x_2, y_2, z_2)$, the locus for CIC tooth profile of the Rotor in the coordinate system $S_2(x_2, y_2, z_2)$ is the same as in Eqs. (4) and (5) and equation of meshing between the driving rotor and driven rotor is presented as in Eq. (6) as follows:

$$\mathbf{r}_{I_2}(\tau, \phi) = \mathbf{M}_{21}(\phi)\mathbf{r}_{I_1}(\tau), \tag{4}$$

$$\text{and } \mathbf{n}_{I_2}(\tau, \phi) = \mathbf{L}_{21}(\phi)\mathbf{n}_{I_1}(\tau), \tag{5}$$

where $\mathbf{L}_{21}(\phi)$ is the upper-left (2×2) sub-matrix of the (3×3) homogeneous coordinate transformation matrix $\mathbf{M}_{21}(\phi)$.

The equation of meshing between the two rotors can be obtained by using Wilson equation

$$(r_p \cos \phi - x_{I_1}(\tau, \phi))x'_{I_1}(\tau, \phi) + (r_p \sin \phi - y_{I_1}(\tau, \phi))y'_{I_1}(\tau, \phi) = 0 \tag{6}$$

The locus for CIC tooth profile of Roots rotor is determined by using Eqs. (1), (2), (3), (4) and (5), simultaneously. The 3D-model of the CIC Roots rotors and 3D-model of two CIC Roots rotor meshing pair are presented in Fig. 2 (b).
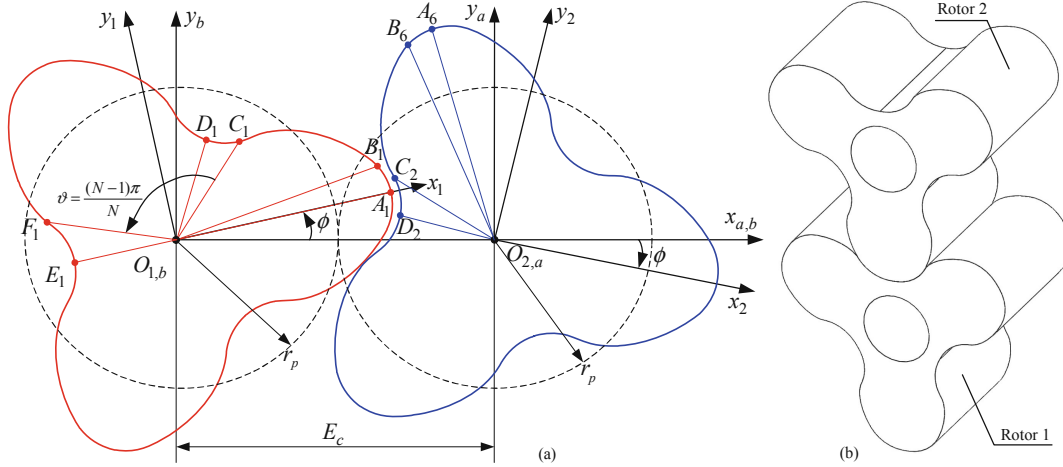
Fig. 2. CIC rotors: a) conjugated coordinate systems and b) 3D meshing rotor pair.

2.2   EE Tooth Profile

The EE tooth profile of rotor is comprised by the epicycloid (A_3B_3) and hypocycloid curves, as shown in Fig. 3. According to Fig. 3(a), the locus tooth profiles of Roots rotor are represented in the coordinate system $S_1(x_1, y_1, z_1)$ as follows:

(1) The extended epicycloid curve A_3B_3:

$$\mathbf{r}_{II_1}^{(A_3B_3)}(\gamma) = \begin{cases} x_{II_1}^{(A_3B_3)}(\gamma) = (r_p + r_e)\cos\gamma + r_e\sin\left(\dfrac{(r_p + r_e)\gamma}{r_e}\right) \\ y_{II_1}^{(A_3B_3)}(\gamma) = (r_p + r_e)\sin\gamma + r_e\cos\left(\dfrac{(r_p + r_e)\gamma}{r_e}\right) \end{cases}, \quad (0 \le \gamma \le \gamma_1) \qquad (7)$$

(2) The hypocycloid enveloped by the epicycloid B_3C_3:

$$\mathbf{r}_{II_1}^{(B_3C_3)}(\gamma) = \begin{cases} x_{II_1}^{(B_3C_3)}(\gamma) = (r_p - r_e)\cos(\dfrac{\pi}{N} - \gamma - \gamma_1) - r_e\cos(\dfrac{\pi}{N} - \gamma + \dfrac{r_p}{r_e}\tau - \gamma_1) \\ y_{II_1}^{(B_3C_3)}(\gamma) = (r_p - r_e)\sin(\dfrac{\pi}{N} - \gamma - \gamma_1) - r_e\sin(\dfrac{\pi}{N} - \gamma + \dfrac{r_p}{r_e}\tau - \gamma_1) \end{cases}, \quad (\gamma_1 \le \gamma \le \gamma_2) \qquad (8)$$

By applying the homogeneous coordinate transformation matrix equation from $S_1(x_1, y_1, z_1)$ to $S_2(x_2, y_2, z_2)$, shown in Fig. 3(a). The locus for EE tooth profile of the Rotor in the coordinate system $S_2(x_2, y_2, z_2)$ is the same as in Eqs. (4) and (5) and equation of meshing between the driving rotor and driven rotor is presented as in Eq. (6). The 3D-model of the EE Roots rotors and 3D-model of two EE Roots rotor meshing pair are presented in Fig. 3(b).
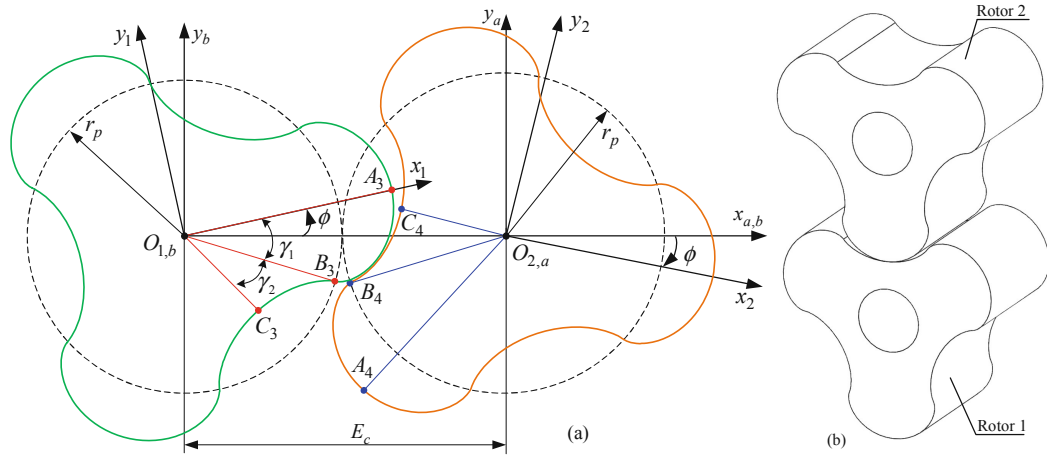
Fig. 3. EE rotors: a) conjugated coordinate systems and b) 3D meshing rotor pair.

3   Contact Force Model

Theoretically, there is no need to distinguish rotor 1 from rotor 2. However, the distinction is often made for numerical convenience, as shown in Fig. 4. The contact condition is the rotor 2 no penetrate into the rotor 1. The contact condition is considered between a node on profile of rotor 2 and a segment on profile of rotor 1. The gap between profile of rotor 1 and profile of rotor 2:

$$g_{ai} = (\mathbf{r}_{p_i} - \mathbf{r}_{q_j}) \cdot \mathbf{n}_i \geq 0 \tag{9}$$

where $\mathbf{r}_{p_i}, \mathbf{r}_{q_j}$ are position vector of rotor profile 1 and rotor profile 2 at points p_i and q_j. If the gap $g_{ai} > 0$, two rotors have no contact and if the gap $g_{ai} < 0$, two rotors have contact.
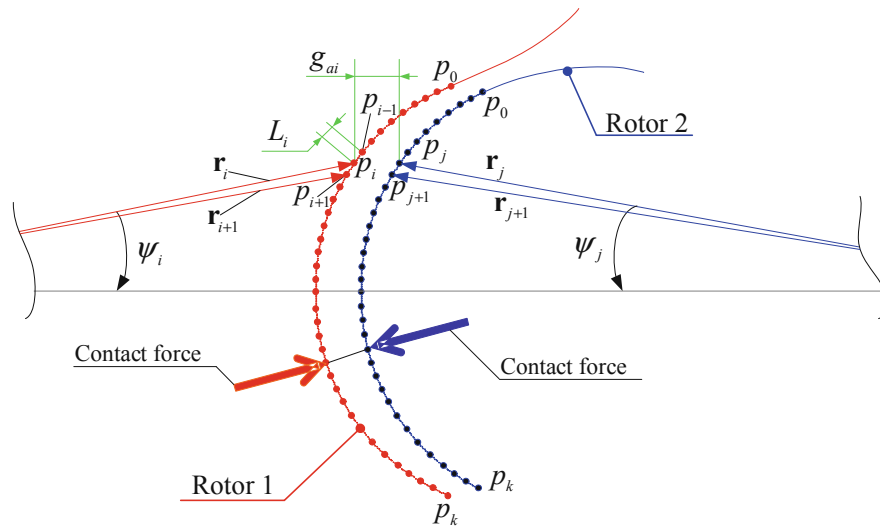

Fig. 4. Gap and contact force between two meshing rotors.

For those contacting rotor pairs, penetration needs to be corrected by applying a contact force and more penetration needs more contact force:

$$F_C = K_n \langle -g_{ai} \rangle \tag{10}$$

where penalty parameter (K_n) is contact stiffness. It depends on material stiffness and allows a small penetration $(g_{ai} < 0)$. A bigger contact stiffness K_n => the less allowed penetration. The proper contact stiffness can be determined from allowed penetration by experience.

4   Numerical Example

In order to determine the contact force between two rotors, the rotors are assembled at a practical center distance of $A_r = 66$ mm. The basic data of the Roots rotor and tooth design parameters are given in Table 1, the contact settings and material properties are given in Table 2 and The input power of rotor is 3 kW and the rotational speed of rotor 3000 rpm. The contact forces are determined for two rotor pairs.

Table 1. Basic data of the root rotor.

Roots rotor		Roots rotor	
Number of rotor lobes (N)	3	Normal pressure angle (α_p)	36.43°
Normal module (m)	22	Center distance (E_c)	66 mm
Pitch radius (r_p)	33.0 mm	Involute parameter (u)	9.00 mm
Outer radius (r_a)	44.88 mm	Top tooth arc angle (θ_1)	4.0°

Table 2. Contact settings and material properties.

Contact settings	
Item	Value
Contact stiffness of the rotors (K_n) (N.mm^{-1})	2.0×10^5
Force exponent (e)	2.2
Damping coefficient of the rotors (C_n)	0.25
Penetration depth (d_s) (mm)	0.01
Material Properties	
Density (kg/mm^3)	7.80×10^{-6}
Elastic modulus (N.mm^{-2})	2.07×10^5
Poisson's ratio	0.29
Coefficient of static friction	0.2
Coefficient of kinetic friction	0.1

The contact force between two EE Roots rotors and two CIC Roots rotors are shown in Figs. 5, 6, 7 and 8. On time domain, the average contact force between two EE Roots rotors, 1047.1 N, is much higher than that of the contact force between two CIC Roots

rotors, 102.4 N. Besides, the maximum contact force between two EE Roots rotors, 5661.4 N, is much higher than that of the contact force between two CIC Roots rotors, 1973.3 N, as shown in Figs. 5 and 6. On frequency domain, the contact force between two EE Roots rotors has much changed extremely abrupt than that of the contact force between two CIC Roots rotors, as shown in Figs. 7 and 8. Therefore, the contact force of CIC Roots rotors have more advantages than that of the EE Roots rotors.
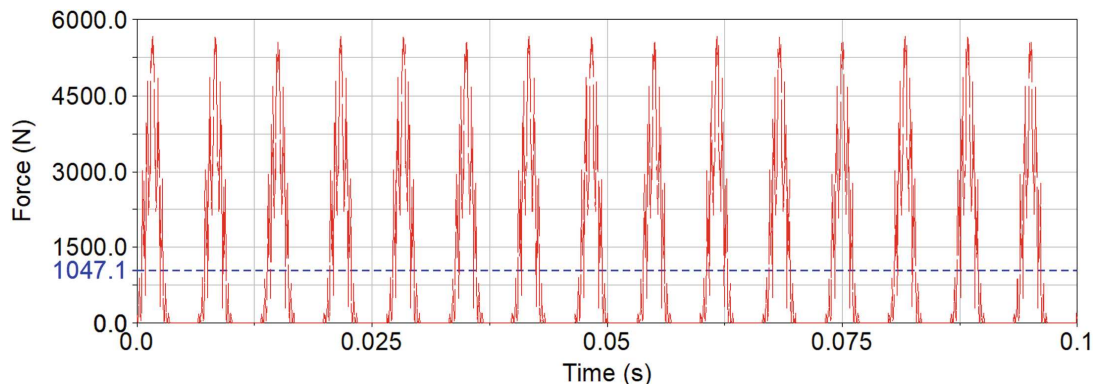

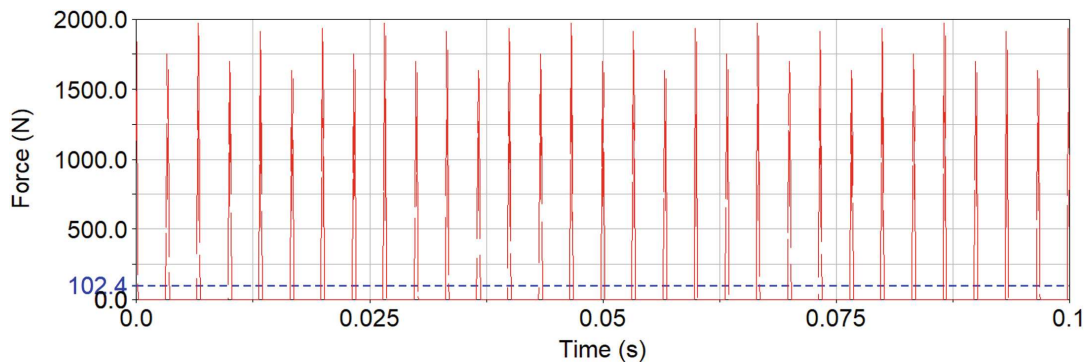**Fig. 5.** The contact force between two EE Roots rotors on time domain.

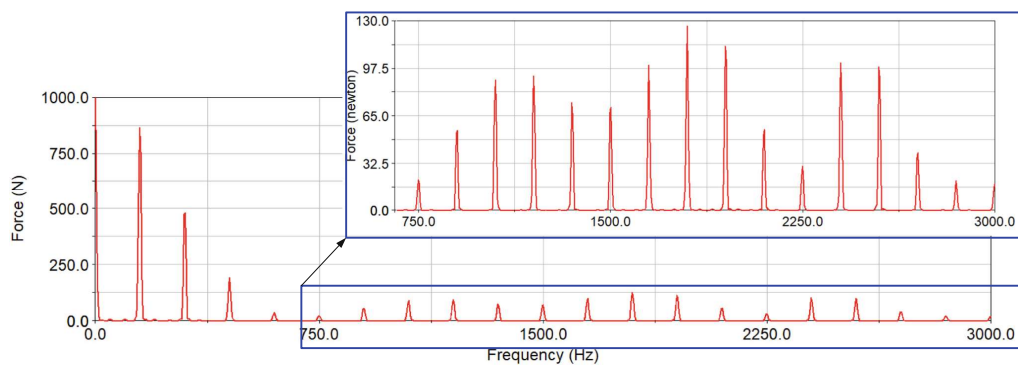**Fig. 6.** The contact force between two CIC rotors on time domain.

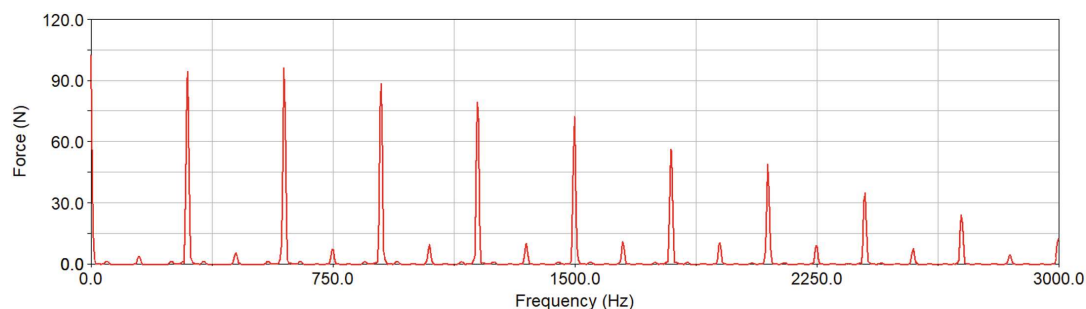**Fig. 7.** The contact force between two EE Roots rotors on frequency domain.

Fig. 8. The contact force between two CIC Roots rotors on frequency domain.

5   Conclusion

In this paper, 3D rotor models for both EE Roots rotors and CIC Roots rotors are constructed. The contact forces of a pair intermeshing rotors are analyzed under combining the torque on the rotor 1 and rotor 2 with the rotation angle of rotor 1. The simulated results show that the contact forces of CIC Roots rotors have more advantages than that of the EE Roots rotors.

References

1. Litvin, F.L., Fuentes, A.: Gear Geometry and Applied Theory, 2nd edn, Cambridge University Press, Cambridge (2004)
2. Tsay, C.B.: Solving the conjugated curves of Roots blower lobe profile by analytic method. J. Machine **13**(1), 129–133 (1987)
3. Vecchiato, D., Demenego, A., Argyris, J., Litvin, F.L.: Geometry of cycloidal pump, computer methods and applied. Mech. Eng. **190**, 2309–2330 (2001)
4. Fang, H.S.: Rotor profile for a Roots vacuum pump, U.S. Patent 5,152,684 (1992)
5. Wang, P.Y., Fong, Z.H., Fang, H.S.: Design constraints of five-arc Roots vacuum pumps. J. Mech. Eng. Sci. Part C **216**(2), 225–234 (2002)
6. Niimura, Y., Kikuta, R., Usui, K.: Two-Shaft type rotary machine having a tip circle diameter to shaft diameter within a certain range, US Patent No. 4943214 A (1990)
7. Hwang, Y.W., Hsieh, C.F.: Study on high volumetric efficiency of the Roots rotor profile with variable trochoid ratio. Proc. Inst. Mech. Eng., Part C-J. Mech. Eng. Sci. **220**(C9), 1375–1384 (2006)
8. Hsieh, C.F., Hwang, Y.W.: Tooth profile of a Roots rotor with a variable trochoid ratio. Math. Comput. Model. **48**, 19–33 (2008)
9. Kang, Y.H., Vu, H.H., Hsu, C.H.: Factors impacting on performance of lobe pumps: a numerical evaluation. J. Mech. **28**(2), 229–238 (2012)
10. Kang, Y.H., Vu, H.H.: A newly developed rotor profile for lobe pumps: generation and numerical performance assessment. J. Mech. Sci. Technol. **28**(3), 915–926 (2014)

11. Chiu, H.C.: The mathematical model and computer aided manufacturing of Roots blower gerotor profile". J. Technol. **9**(1), 13–19 (1994)

12. Tran, V.-T., Thanh, B.T., Long, B.T., Tuan, H.Q., Toan, N.D.: Study on the effects of tooth profile design parameters of rotor to performance of vacuum pump. Int. J. Modern Phys. B, 2040141 (2020). https://doi.org/10.1142/s0217979220401414